2015

# Temporally and Spatially Resolved Plasma Spectroscopy in Pulsed Laser Deposition of Ultra-Thin Boron Nitride Films

Nicholas R. Glavin
*Air Force Research Laboratory*

Christopher Muratore
*University of Dayton*, cmuratore1@udayton.edu

Michael L. Jespersen
*University of Dayton*, mjespersen1@udayton.edu

Jianjun Hu
*University of Dayton*, jhu001@udayton.edu

Timothy S. Fisher
*Purdue University*

***See next page for additional authors***

# Temporally and spatially resolved plasma spectroscopy in pulsed laser deposition of ultra-thin boron nitride films

Nicholas R. Glavin,[1,2,a)] Christopher Muratore,[1,3] Michael L. Jespersen,[1,4] Jianjun Hu,[1,4] Timothy S. Fisher,[2] and Andrey A. Voevodin[1,a)]
[1]*Materials and Manufacturing Directorate, Air Force Research Laboratory, Wright-Patterson AFB, Ohio 45433, USA*
[2]*School of Mechanical Engineering and Birck Nanotechnology Center, Purdue University, West Lafayette, Indiana 47907, USA*
[3]*University of Dayton, Dayton, Ohio 45409, USA*
[4]*University of Dayton Research Institute, Dayton, Ohio 45409, USA*

(Received 6 March 2015; accepted 11 April 2015; published online 24 April 2015)

Physical vapor deposition (PVD) has recently been investigated as a viable, alternative growth technique for two-dimensional materials with multiple benefits over other vapor deposition synthesis methods. The high kinetic energies and chemical reactivities of the condensing species formed from PVD processes can facilitate growth over large areas and at reduced substrate temperatures. In this study, chemistry, kinetic energies, time of flight data, and spatial distributions within a PVD plasma plume ablated from a boron nitride (BN) target by a KrF laser at different pressures of nitrogen gas were investigated. Time resolved spectroscopy and wavelength specific imaging were used to identify and track atomic neutral and ionized species including $B^+$, B*, $N^+$, N*, and molecular species including $N_2$*, $N_2^+$, and BN. Formation and decay of these species formed both from ablation of the target and from interactions with the background gas were investigated and provided insights into fundamental growth mechanisms of continuous, amorphous boron nitride thin films. The correlation of the plasma diagnostic results with film chemical composition and thickness uniformity studies helped to identify that a predominant mechanism for BN film formation is condensation surface recombination of boron ions and neutral atomic nitrogen species. These species arrive nearly simultaneously to the substrate location, and BN formation occurs microseconds before arrival of majority of $N^+$ ions generated by plume collisions with background molecular nitrogen. The energetic nature and extended dwelling time of incident $N^+$ ions at the substrate location was found to negatively impact resulting BN film stoichiometry and thickness. Growth of stoichiometric films was optimized at enriched concentrations of ionized boron and neutral atomic nitrogen in plasma near the condensation surface, providing few nanometer thick films with 1:1 BN stoichiometry and good thicknesses uniformity over macroscopic areas. © *2015 AIP Publishing LLC*. [http://dx.doi.org/10.1063/1.4919068]

## INTRODUCTION

The nano-scale miniaturization of electronic components has led to recent advances in synthesis techniques of atomically thin two-dimensional (2D) materials for the possibility of constructing functional, flexible, and tunable devices from their heterostructures.[1–3] While significant progress has been made in synthesis techniques for conducting 2D materials, such as graphene, and semiconducting materials, such as transition metal dichalcogenides,[4,5] reliable synthesis methods for insulating materials in the 2D form is relatively unexplored. Boron nitride (BN), an atomically thin 2D material consisting of alternating boron and nitrogen atoms in a hexagonal lattice structure similar to graphene, exhibits an intrinsic band gap near 5 eV, making BN an attractive dielectric for graphene-based device structures. Despite the promise as a 2D dielectric material, the mechanisms underlying the synthesis of the ultra-thin films by physical vapor deposition (PVD) have not been systematically investigated.

Recent work has shown that pulsed laser deposition (PLD) techniques can facilitate the formation of stoichiometric few layer thick 2D hexagonal BN films on lattice matched substrates, and amorphous, dense films with aspect ratios equivalent to that of crystalline 2D films (e.g., $>10^6$ length/thickness) on non-lattice matched substrates over few square centimeters areas.[6] The kinetic energies of the species within the plasma sheath created by PLD enable significant atomic mobility on substrate surfaces, leading to nanocrystalline growth at temperatures 300 °C lower than that required for comparable chemical vapor deposited (CVD) films. The ability to grow nanoscale insulating films at reduced processing temperatures and on wafer-scale areas gives the potential for compatibility with numerous 2D semiconductor material systems and, hence, provides for an attractive, alternative growth method for integration of boron nitride into nanoelectronic device architectures.

Several earlier studies of laser ablated plasmas from boron nitride targets were directed towards the understanding of crystal formation and chemistry of boron nitride films in the amorphous, hexagonal, and cubic phases. Wei *et al.*[7] were one of the first to investigate the time of flight and velocity of ionized boron ($B^+$) species expelled from a BN

a)Authors to whom correspondence should be addressed. Electronic addresses: nicholas.glavin.1@us.af.mil and andrey.voevodin@us.af.mil

 

target during ablation by optical emission spectroscopy in a wavelength range from 300–600 nm. Discovery of atomic $B^+$ velocities close to the target exceeding $10^5$ cm/s led to the hypothesis that this species is critical in BN thin film formation. Murray *et al.*[8] and then Doll *et al.*[9] both expanded on this by incorporating mass spectroscopy time of flight studies of the $B^+$ ions and a more detailed optical emission spectroscopy at similar wavelengths, respectively. In the study by Murray *et al.*, the formation of stoichiometric BN in an $NH_3$ environment was linked to the abundance of ($B^+$) and ($N^+$) with a hypothesis on BN formation in gas phase based on the cluster detection by mass-spectroscopy. Additional time of flight and optical spectroscopy studies at different nitrogen background gas pressures and laser powers were conducted by Shin *et al.*[10] and by Angleraud *et al.*[11] These studies confirmed that the plumes consist mainly of neutral and ionized atomic boron with a presence of ionized atomic nitrogen, while the presence of molecular BN in the plasma plumes is negligible. The studies also reported plume confinement and deceleration by collisions with background nitrogen gas, changing BN plume behavior from earlier stage direct propagation to a shockwave formation and hydrodynamically controlled propagation at later stages in plume development.[11] In a more recent paper by Dutouquet *et al.*,[12] the focus was on identification of BN radicals in the 340–390 nm emission window of the laser ablated plumes, where the presence of BN was identified but the overall intensity in comparison to atomic emissions was fairly low. These earlier studies clearly highlight the significance of the background gas pressure on the shockwave formation and plume propagation dynamics, plasma plume composition, and possible reaction mechanisms for the film growth.

Most of these earlier plasma studies were directed towards the appropriate growth conditions required for the cubic phase of boron nitride, as the extreme hardness, high thermal conductivity, and chemical stability make this phase of BN attractive for certain industrial applications including erosion, oxidation resistance, and wear protective coatings.[9,13–15] For cubic BN phase formation, the utilization of high kinetic energy of laser ablated B and N species were critical, which their translational velocities were reported as high as 20–50 km/s depending on the background nitrogen pressure.[11] Observations of nitrogen specie chemistry at the substrate location and reactions at the substrate surface due to plume collisions with background gas and condensation surface were explored to a lesser degree. Only recently have hexagonal and amorphous phases at the nanoscale thickness scale become of comparable interest[16] for application to electronic and optoelectronic devices. In order to facilitate nanoscale, stoichiometric BN thin film growth, optimization of incoming plasma species composition and energies at the substrate/condensate interface is necessary to aid in the formation of stoichiometric BN while avoiding deterioration under the excessive bombardment by energetic ablated plume species. In this study, plasma spectroscopy over a wide wavelength range and plasma imaging at the substrate location have been utilized to elucidate mechanisms that promote nucleation and growth of ultra-thin stoichiometric and uniform BN films by PLD.

## EXPERIMENTAL DETAILS

A detailed schematic of the experimental deposition chamber configuration has been published previously.[6] Laser ablation occurred from a Boron Nitride target (99.99% pure) at a square area of 2.66 mm × 1.50 mm, using a KrF LPX Lambda Physik excimer laser. At 900 mJ/pulse, the single pulse energy was 22 J/cm$^2$, pulse width of 30 ns, and repetition rate of 1 Hz. The residual base pressure was $2.0 \times 10^{-9}$ Torr within the chamber, which was filled with high purity nitrogen gas (99.9999%) at pressures between 5 and 100 millitorr (mTorr). The working distance between substrate and target was approximately 3.5 cm, and the substrate holder was maintained within the chamber at a constant position during all spectroscopy studies. A large glass window was used as a viewport (transmittance cutoff 300 nm) for both plasma imaging and spectroscopy data collection.

Spectroscopic analysis was performed on two distinct regions within the ablated plumes to evaluate plasma compositions both close to the target (Region 1) and adjacent to the substrate (Region 2), as in Figure 1. A focusing lens assembly coupled to a fiber optic guide focused the collected area to approximately 2.5 cm in diameter. The fluorescent light was captured by adjusting the slit width between 1 and 20 $\mu$m at the entrance of an Acton Research Spectra Pro 150 monochromator connected to a high speed Princeton Instruments 576-S/RBE image intensified charge-coupled device (ICCD) detector. The spectrometer was calibrated using a HeNe light source and maintained a calibration threshold of ±0.1 nm across the spectrum window and in the high resolution scans. A 1200 l/mm grating and a 150 l/mm grating allowed for collection of both high resolution spectra at narrower wavelength windows, and lower resolution spectra at broader windows, respectively. Broad spectra of Regions 1 and 2 were initially accumulated upon laser impact on the target and extended to 10 $\mu$s, which was well after any residual plasma emission was detected in either region. Time of flight measurements were performed with the use of a gated pulse generator (Princeton Instruments Model PG-200) at a 200 ns delay from the laser pulse, and high resolution spectra were collected at increments of 200 ns steps and a 200 ns gate width. High resolution spectra were taken at each 200 ns increment for intensity measurements. Peak identification was

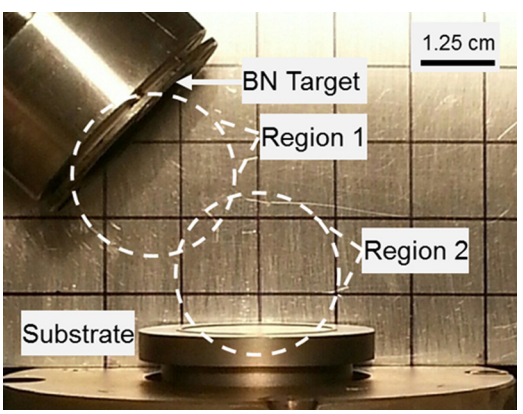


FIG. 1. Image inside growth chamber indicating locations for BN target, substrate, and two collection regions used for spectroscopic analysis.

completed by comparing to spectral lines of atomic excited species in the NIST database[17] and molecular band spectral lines of characteristic $N_2$ and BN emission systems.[18] Plasma images were captured using a focus zoom lens coupled to the ICCD detector array and each image corresponds to an individual laser pulse. Narrow bandpass filters (10 nm FWHM) were used for isolation of atomic nitrogen gas emissions (400 nm and 750 nm filter) for imaging, each with a transmittance of approximately 50%.

The numerical intensity values accumulated via spectroscopy techniques are dependent on multiple variables including the spectroscopic data collection setup (i.e., slit width, gain on the detector, gate width, and timing mechanism), the Einstein coefficient of the electron transition (rate of photons emitted/time), the concentration of atomic species, the probability of a given electron transition state, and the dwell time of that species within the spectroscopic collection window. Thus, in all comparative studies, the camera and spectrometer settings remained constant within that data set to allow for direct relative comparison of plasma emission phenomena. Scans within each data set were performed in succession, and the target was re-polished frequently to avoid any surface morphology changes which can alter the ablation plume dynamics.

Ultra-thin, amorphous boron nitride films were grown at room temperature on 5 mm × 5 mm sapphire [0001] polished substrates at 5, 50, and 100 mTorr background pressure and 10 laser pulses. In the growth experiments, five samples were placed adjacent to one another and normal to the target orientation and at a location in which the front of the plasma plume directly impacts the center of the five sample assembly (sample position 3). In this setup, each sample location advances 5 mm on the substrate surface away from the target, covering a total distance of 25 mm from sample position 1 to 5. X-ray photoelectron spectroscopy techniques were used to evaluate both chemical compositions and thicknesses of films deposited at different sample locations and background gas pressure conditions. XPS experiments were conducted using a Kratos AXIS Ultra spectrometer with a monochromatic Al Kα x-ray source (1486.67 eV) operated at 120 W (12 kV, 10 mA) under ultra-high vacuum conditions ($\sim 2\times 10^{-9}$ Torr). In this system, the analyzer is oriented at 90° relative to the sample surface. Survey scans were collected over the binding energy range of −5–1200 eV, in 1 eV steps, using a dwell time of at least 500 ms and analyzer pass energy of 160 eV. High resolution spectra of the B *1s*, N *1s*, O *1s*, and C *1s* regions were acquired using an energy step size of 0.1 eV, a dwell time of 500 ms, and analyzer pass energy of 20 eV. A low-energy electron flood source was utilized for charge compensation. XPS spectra were analyzed using the CasaXPS software. Peak areas were determined using a Shirley background subtraction and were corrected by the appropriate relative sensitivity factors to obtain elemental composition. Film thickness estimations utilizing XPS data were based upon the exponential decay of substrate photoelectrons with increasing overlayer thickness due to inelastic scattering effects. Atomic concentration ratios between unique, non-interfering photoelectron peaks from the overlayer (B *1s* or N *1s*) and the substrate (Al *2p*) were fit to a model incorporating the inelastic mean free paths (IMFPs) of substrate photoelectrons within the substrate and within the BN layer, in addition to photoelectrons originating from within the BN layer in order to determine an effective film thickness.[19] IMFP values were estimated using the NIST-71 Database.[20] XPS measurements of thin film thickness were additionally verified with cross sectional transmission electron microscopy (TEM) imaging.

## RESULTS AND DISCUSSION

Emission spectra collected at two specific regions between the target and substrate indicate differences in energies and compositions due to collisions of the ablated plasma species with the background gas during initial formation and transport of the plume within the growth chamber. Localized pressure and temperature increases due to rapid evaporation of target material, typical of those observed in pulsed laser deposition experiments, cause the formation of species including ionized boron $B^+$ (345.1 nm) and $B^{2+}$ (448.7 nm), ionized nitrogen $N^+$ (395.5 and 399.5 nm), and lesser emitting excited neutral species B* (582.1 nm) and N* (748.6 nm), as shown in Figure 2. The background gas composition and pressure had little influence on the emission spectra close to the target surface because collisional interactions with the nitrogen gas are limited, as the plasma is initially confined within dense adiabatically expanding ablated plume and observed excitations originate from species formed from the BN target. In particular, support of this assertion is the observation that the spectra in this region do not indicate the presence of molecular nitrogen in either the vacuum or gas case. The presence of a doubly ionized $B^{2+}$ species is unique to this region close to the target surface, and has been observed in other ablated BN plasmas[11] when laser energies exceed 20 J/cm$^2$. These $B^{2+}$ ions have a short life time and recombine quickly with plasma electrons, forming the more stable $B^+$ species. Plasma images shown in the inset of Figure 2 depict the similarities in emission intensities and spatial distributions of the plasma at the first 600 ns after the

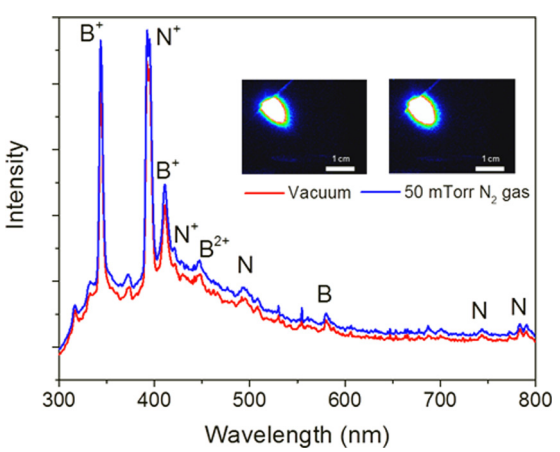


FIG. 2. Broad spectra from Region 1 of ablated plasma from a BN target in vacuum and in 50 mTorr nitrogen gas; and the inset images depict plasma emission 600 ns after the laser interacts with the target at the indicated pressures.

laser pulse when the majority of the plasma is still within the Region 1 collection area.

In the collection region adjacent to the substrate surface (Region 2 in Figure 1), the plasma plume experiences changes in energies and compositions as the pressure within the chamber increases. In ultra-high vacuum conditions, the accelerated ablated particles travel quasi-ballistically from target to substrate, as the mean free path for collisional interactions is much larger than the distance between target and substrate. As molecular nitrogen species are added to the chamber, a much shorter mean free path and an increased probability of multiple collisional interactions are expected. As indicated in Figure 3, many of the emitted species are common in both the vacuum and gas conditions; however, the peak height of the emission intensities is about an order of magnitude higher with the inclusion of a background gas at a pressure of 50 mTorr (scale bars in Figure 2 for vacuum and 50 mTorr spectra represent 10 000 counts and 100 000 counts, respectively). This change is due to the plume confinement within the collection region, resulting in a longer dwell time and more collisional excitations of ablated species with the nitrogen background gas.

Plasma images in Figure 2 also display the confinement of the plume in the collection window and very different plasma distribution at longer times after the laser pulse and in the region close to the substrate surface. The presence of ionized atomic boron $B^+$ (317.93 and 345.1 nm) and ionized atomic nitrogen $N^+$ (395.5, 399.5, 422.8, 594.3 nm) dominates the spectra upon the inclusion of nitrogen background gas, as both long-lived species are able to retain their ionization within the collection window at a high concentration. The strongest peaks in the spectrum belong to singly ionized boron and ionized nitrogen, but the contribution to neutral nitrogen is stronger than that of neutral boron, as the presence of excited neutral boron B* (582.1 nm) and nitrogen N* (648.5, 742.4, 744.3, 746.8, 818.5, 820.0, 821.1, 827.6, 822.3, 822.2, and 868.12 nm) are observed mostly in the near-infrared. The presence of the neutral excited nitrogen species is unique to this wavelength region, as many other spectroscopic studies of BN ablated plasma do not report this species in any other frequency range. The first ionization potential for metallic boron of 8.3 eV minimizes the concentration of neutral boron, as the ionization process in high energy plasmas occurs fairly easily. The more electronegative nitrogen is known to have a higher ionization energy of 14.5 eV, which results in the larger number of peaks of the neutral nitrogen than the neutral boron. Unlike region 1, the presence of the doubly ionized species of boron is absent, as the energy required for this ionization is 25.2 eV, more than three times higher than the first ionization energy. Molecular neutral and ionized molecular nitrogen gases, $N_2$ (313.6, 315.9, and 337.1 nm) and $N_2^+$ (391.4, 423.7, and 427.8 nm), respectively, are observed, but only in the presence of a background gas and are not observed in the vacuum condition.

A comparison of emission intensities for several species at both the vacuum condition and in the presence of 50 mTorr of nitrogen is shown in Figure 4. The comparisons are that of high-resolution spectra taken in a small wavelength window, to allow for precise determination of peak height and location. The changes in intensity upon the addition of a background gas vary significantly as the individual species are impacted differently based on the predominant decay mechanisms and confinement behavior. The ionized boron and neutral excited boron ($B^+$ and B*) intensities increase

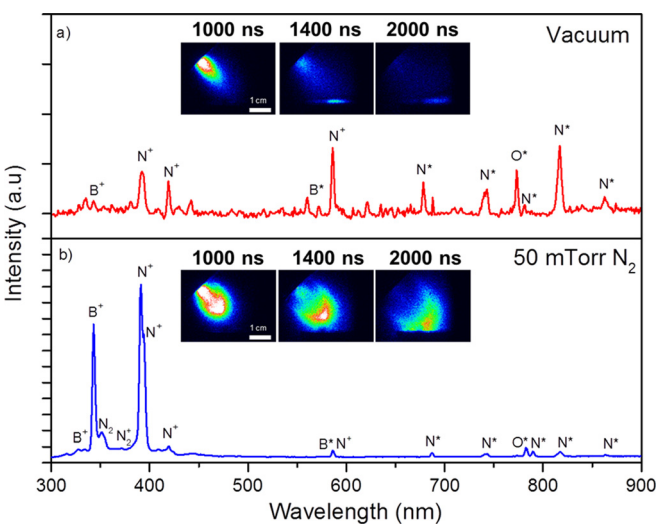


FIG. 3. Broad spectra from Region 2 of ablated plasma in (a) vacuum and (b) 50 mTorr. The scale bars for vacuum and 50 mTorr spectra are 10 000 counts and 100 000 counts, respectively. The inset of each graph displays plasma imaging of full spectra as a function of time after the laser pulse for each corresponding pressure condition.

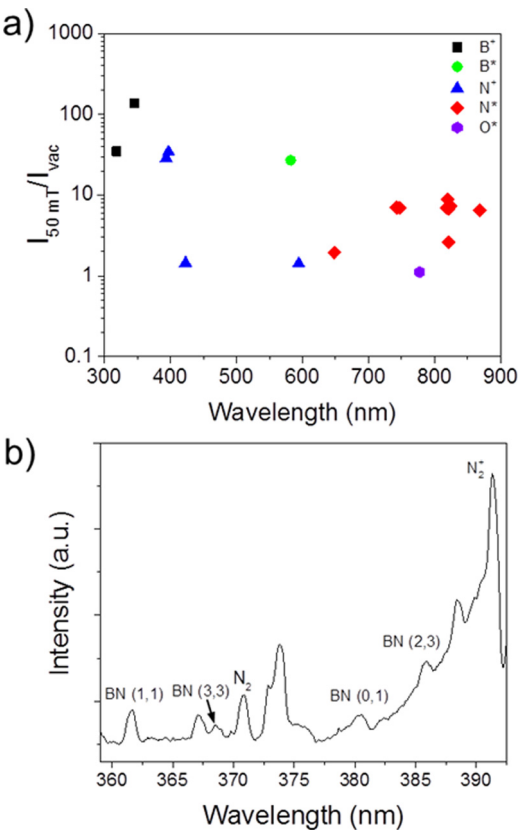


FIG. 4. (a) Peak height intensity ratio in 50 mTorr background gas to vacuum of the major identified plasma species, and (b) high resolution spectra of observed BN radicals at 2600 ns after laser pulse.

by at least an order of magnitude, and in the case of the dominant $B^+$ peak at 345.1 nm, an increase of more than 100 times is observed. In the case of neutral excited nitrogen (N*), the change in intensity of emission is not as significant as that of the boron species. With an average ratio of intensity at 50 mTorr to that of vacuum of 7 times, the intensity of gaseous neutral excited nitrogen emission is clearly less affected by the background gas confinement than in the case of the boron atomic species.

The ionized nitrogen atomic species appears to behave in a different manner depending on which wavelength peak is identified. At 399.5 nm and 395.5 nm, the intensities are 20 times greater in gas than in vacuum, and at 422.7 and 594.3, the intensity ratios are nearly unity. The observed difference in the ratio of intensities is hypothesized to occur because of the different creation and decay mechanisms for this particular emitting species, as some formation of $N^+$ is due to ablation from the target material, and the rest from the dissociation reactions of $N_2$ gas interacting with energetic electrons and other nitrogen species, which will be discussed in more detail later. In addition, the energetic $N^+$ formed by the laser ablation process will have much higher energy than that formed from dissociation of the background gas within the chamber. It is important to note that there is a small amount of emission assigned to the neutral excited oxygen present in the target material. The presence of oxygen in Region 2 is small, and the intensity does not change as the background gas is added, indicating that the flight of oxygen from the target to the substrate is similar in both cases. Oxygen is a well-known contaminant in boron nitride systems, and has been observed in other ablation plasmas from similar boron nitride targets.[21]

The primary band system $A^3\Pi \rightarrow X^3\Pi$ of the BN molecule, occurring between 340 and 400 nm, has relatively weak emission intensity compared to the atomic emission, and can be further masked by intense peaks of ionized boron at 345.1 nm and the second positive system $C^3\Pi \rightarrow B^3\Pi$ of excited molecular nitrogen $N_2$ from 350 nm to 400 nm. This has led to assumptions that the recombination reaction to form BN is not dominant in the plasma[11] and likely to occur at the substrate surface.[9] In selected cases, including this study, observation of the boron nitride radical can be resolved. Figure 4(b) shows a high resolution spectrum of several resolved BN peaks between 360 and 385 nm at 2600 ns after the laser pulse and in 50 mTorr of nitrogen. The observed vibrational transitions of BN match fairly well with similar molecular peaks reported by Dutouquet *et al.*[12] ($\nu' = 1$, $\nu'' = 1$ at 362.5; $\nu' = 3$, $\nu'' = 3$ at 368.2 nm; $\nu' = 0$, $\nu'' = 1$ at 380.3; and $\nu' = 2$, $\nu'' = 3$ at 385.6 nm). In the vacuum condition, the BN radical presence was not detected.

Time of flight measurements of the intensity of major peaks associated with $B^+$ (345.1 nm), $N^+$ (395.5 nm), N* (748.8 nm), and $N_2^+$ (391.4 nm) in Region 2 at background pressures from 5 mTorr to 100 mTorr are shown in Figure 5. The formation and decay mechanisms for each emitting species change as collisional interactions with the background gas alter plasma energies, concentrations, temperatures, and dwell times within the collection region. Ionized boron, $B^+$, is formed solely from the target ablation and ionization of small amount of neutral boron in the plasma plume. Boron, being the lighter of the two species (atomic weights: B = 10.81, N = 14.01), will escape the Knudsen layer of plasma plume at higher velocity and reach the surface before the neutral or ionized nitrogen. However, the atomic radius of the boron is larger than that for nitrogen, as the collisional cross section is approximately 31% larger. The larger radius, low ionization energy, and the fact that the only creation mechanisms in the plasma are from ionization of neutral boron and from the ablation process result in a maximum in boron emission intensity at the substrate at a pressure of 50 mTorr. At pressures less than 50 mTorr, the ionized boron species move quickly towards the substrate and are dispersed quickly. The electron density at gas pressures approaching 50 mTorr is sufficient to maximize the number of $B^+$ ions. At pressures higher than 50 mTorr, the plasma system is becoming depleted of electrons, in part from the dissociative recombination reaction as discussed later, and the plume begins to become thermalized, reducing the concentration of ionized boron. From the maximum locations in time of flight data in Figure 5(a), kinetic velocity of the majority of the $B^+$ species arriving at the substrate was found to decrease from about 35 km/s at 5 mTorr pressures to 22 km/s at 100 mTorr, indicating the collisional deceleration of $B^+$ species in background gas. These estimated average speeds are consistent with that reported in the early studies for BN ablation in nitrogen background.[11]

The near substrate emission from atomic neutral nitrogen species, N*, increases with background pressure, and reaches a maximum at pressures around 50 mTorr. Beyond that pressure, the confinement of the plume is enough to restrict propagation of the N*, as well as increase the reaction time with the ionized boron to form BN at the interface. Unlike the ionized boron species at higher pressures, the maximum intensity of N* saturates beginning around 50 mTorr and the maximum location is not considerably shifted with the increased pressure. This indicates that in addition to atomic nitrogen generated from the target surface, a significant contribution is also due to dissociation and ionization of the background nitrogen in collisions within the shockwave front of the plasma plume, which formation is confirmed for pressures above 30 mTorr from plasma plume imaging studies discussed later.

Ionized atomic nitrogen is the longest living emitting species characterized within the plasma system, as the decay mechanism is dominated entirely by impact with the substrate and chamber walls.[22] The peak emission time for this species is nearly 600 ns after the peak emission time for both neutral nitrogen and ionized boron. Competing mechanisms for the formation of the ionized nitrogen include species formed from the ablation process, separation of $N_2$ directly to $N^+$ from a high energy collision, ionization of neutral nitrogen, secondary ionization from collisions with the substrate, and the following gas dissociation reactions:

$$N_2 \rightarrow N_2^+ + e^-; \quad (1)$$

$$N_2^+ + e^- \rightarrow 2N; \quad (2)$$

$$2N \rightarrow 2N^+ + 2e^-. \quad (3)$$

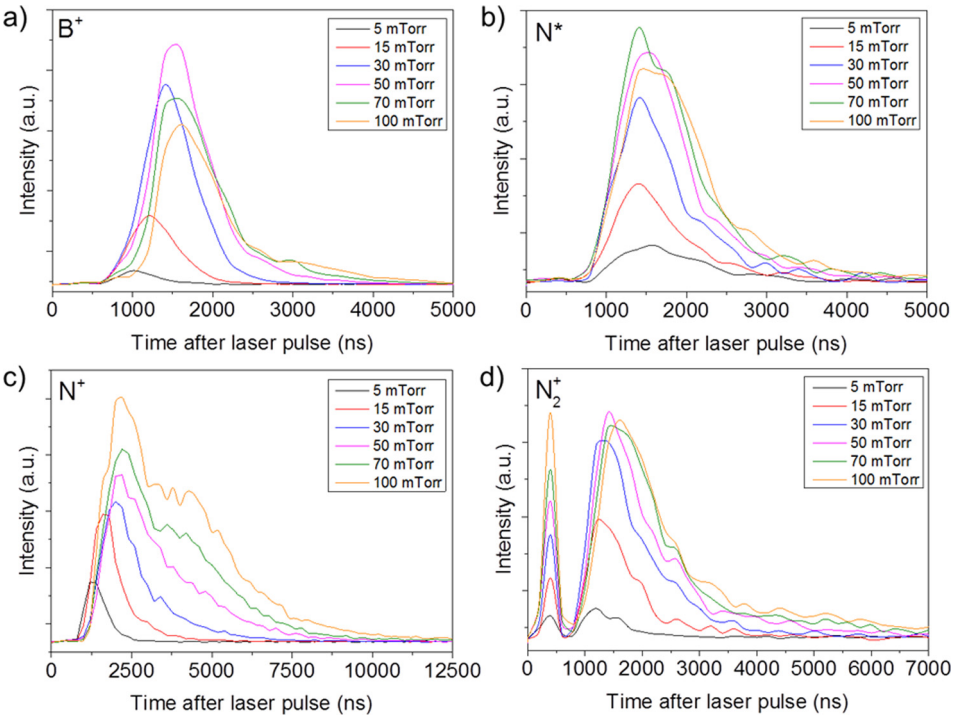


FIG. 5. Time of flight intensities for (a) $B^+$ (345.1 nm), (b) N* (748.8 nm), (c) $N^+$ (395.5 nm), and (d) $N_2^+$ (391.4 nm) peaks in Region 2 from ablation of a BN target.

The proposed reaction mechanism occurs readily in the nitrogen plasma as collisions with electrons, atomic, and molecular species at high energies cause decomposition of molecular nitrogen and quickly form atomic nitrogen, which then lose an electron and form ionized nitrogen. The ionization mechanisms described in Refs. 1 and 3 occur fairly rapidly at high electron densities. In addition, the dissociative recombination reaction in Ref. 2 has an extremely high reaction rate of $\sim 1 \times 10^{-7}$ cm$^3$ s$^{-1}$, and thus, the mechanism described here dominates over other possible molecular nitrogen dissociations.[23] Emission from ionized nitrogen in Region 2 can be detected only as the neutral nitrogen and ionized boron emission maximize within the same region, at around 1400 ns, as much of the formation of $N^+$ is due to the dissociation reaction of molecular nitrogen species.

Molecular emission from ionization of background gas has a strongest band for the transition $B^2\sum_u{}^+ \rightarrow X^2\sum_g{}^+$ ($\nu' = 0$, $\nu'' = 0$) of $N_2^+$ at 391.4 nm is shown in Figure 5(d). A large emission peak at 400 ns after the laser pulse is consistent in time for the entire pressure range tested in this study, and increases as the pressure and concentration of gas within the chamber increases. This may be caused by high electron density at the leading edge of the plasma plume that travels collisionlessly to the substrate location, leading to further excitation of the background gas species as they propagate from target to substrate. The leading edge electron densities in laser ablated plasma can be as high as $10^{20}$ electrons/cm$^3$, which can be greater than the density very close to the target during ablation.[24] After the leading edge excitation occurs in the background gas at around 400 ns, the main plasma plume flux causes ionization just before 1000 ns. The intensity of ionized molecular nitrogen increases as the gas pressure within the deposition chamber increases and reaches a maximum at values greater than 30 mTorr and at a time of 1600 ns. At pressures higher than 30 mTorr, the behavior of the emission from the ionized molecular nitrogen is very similar up until 100 mTorr, even though the concentration of nitrogen gas is higher. This indicates that above 30 mTorr, a transition of plasma plume to a collisional dissociation and recombination process equilibration occurs, which is also linked to an expected transition from direct plume propagation to confined propagation and a shock wave front generation at increased nitrogen background pressure.[11]

The peak time of emission for the atomic species, shown in Figure 6, is directly dependent upon background gas pressure for the ionized species, and appears nearly independent for the neutral nitrogen. At 50 mTorr background gas, the peak emission time for the ionized boron and ionized nitrogen reach a constant at 1600 ns and 2200 ns, respectively. The energy and reaction mechanisms within the plasma at 50 mTorr appear to optimize the peak emission time for all of the participating reaction species detected by emission

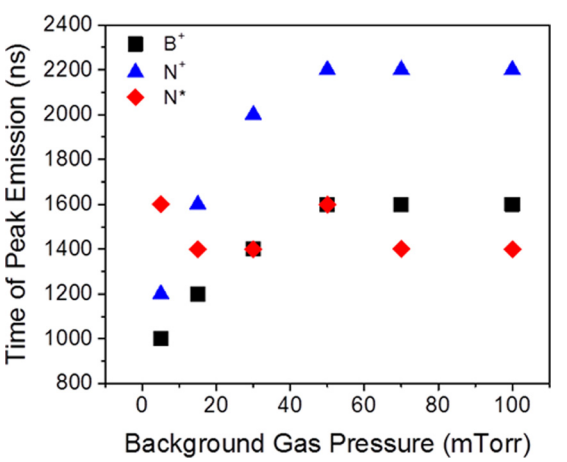


FIG. 6. The time of the most intense emission for each of the atomic species as the background gas pressure in the chamber increases.

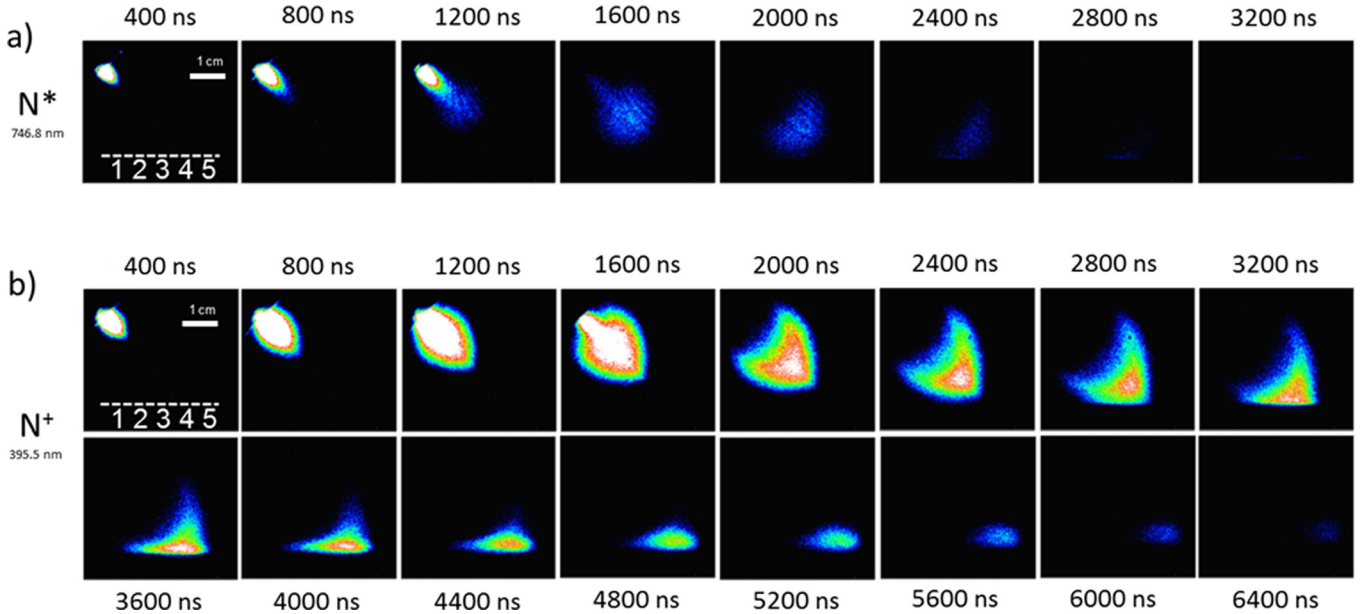


FIG. 7. Plasma imaging through narrow bandpass filters for (a) N* at 746.8 with a 750 nm filter, and (b) $N^+$ at 395.5 nm with a 400 nm filter at 50 mTorr background gas pressure. The dotted line indicates the location of the substrate and numbers indicate locations of the sapphire (0001) samples.

spectroscopy, as pressures beyond that will saturate the reaction behavior. This observation is further demonstrated by the plasma intensity ratios (Figure 4(a)), as the ionized species tend to be much more affected by the presence of the background gas, and the emission from neutral species is not as influenced.

Spatial emission plasma images of the plume propagation at 50 mTorr pressure appear in Figure 7. Narrow bandpass filters of 750 nm and 400 nm isolate the observed plasma emission to just the individual N* and $N^+$, respectively. Both species exhibit similar emission behavior shortly after the laser pulse, where the plume is close to the ablation target and is not significantly impacted by the background gas collisions. As the plume begins to form and move toward the substrate location, the atomic neutral nitrogen within the plasma is centralized within the plume and is extinguished as it reacts within the plasma and hits the interface with the substrate, most likely forming BN. The shape of the N* and $N^+$ distributions in the plasma plume is much different. The exited neutral nitrogen profile is quickly transitioning from a high intensity and directional plume shape to a relatively weak and strongly confined distribution, which is mostly extinguished by 2800 ns time at arriving to the substrate location Figure 7(a). In contrast, the $N^+$ emission imaging exhibits a clear transition to a reverse cone-shaped distribution and formation of a hemispherical shock front (Figure 7(b)), which is typical for plasma plumes undergoing collisional decelerations in background gas.[25]

From the comparison of Figures 7(a) and 7(b), the ionized nitrogen presence considerably lags behind the neutral nitrogen, indicating that the formation of $N^+$ is primarily from the dissociation and ionization of the background gas caused by the collisions with species in the ablated plume. While the majority of the $N^+$ is extinguished upon impact with the substrate surface, some deflects and forms a sheath over the far end of the substrate location. This creates an additional extended presence (beyond 6000 ns) of ionized high energy nitrogen at the substrate surface as it diffuses through the plasma sheath.[22] The high energy collisions with substrate can cause desorption of the deposited film and lead to re-ionization of nitrogen species, further extending the lifetime of the plasma sheath at the film growth surface.

Plasma spectroscopy results from BN laser ablation processes were correlated to fundamental mechanisms of thin film nucleation and growth. Figure 8 displays the BN ratio and thickness, as measured by XPS, of five sapphire samples placed at different distances from the target as shown by the inset. The ratio of boron to nitrogen is critical in material performance, as films with a B:N ratio greater than 1 indicate a significant amount of metallic bonding and nitrogen vacancies, and a B:N ratio less than 1 can lead to nitrogen trapped in the film or the presence of NO. An increase in the B:N ratio with distance indicates a decrease in the nitrogen content in the films at locations further from the target. Also, the increase in background pressure leads to a decrease in the BN ratio, with a near-optimum BN ratio at position 3 at 50 mTorr.

The pressure of 50 mTorr and sample position 3 marked in Figure 8(a) is also an optimum for the extended presence of the plasma plume at the substrate surface location. Evident in the bandpass filter plasma images, the further positions (4 and 5 in Figure 8(a) have much less plasma reaction time with boron and neutral nitrogen, while exposed to a significant and extended amount of ionized nitrogen. Indicated in Figure 7(b), the ionized species $N^+$ resides near position 4 and 5 for at least a period of 2000 ns. It is hypothesized that the neutral nitrogen plays a much greater role in formation of BN films, as concentration of neutral nitrogen at positions 4 and 5 is much depleted. In addition, the neutral nitrogen will arrive at the substrate before the ionized

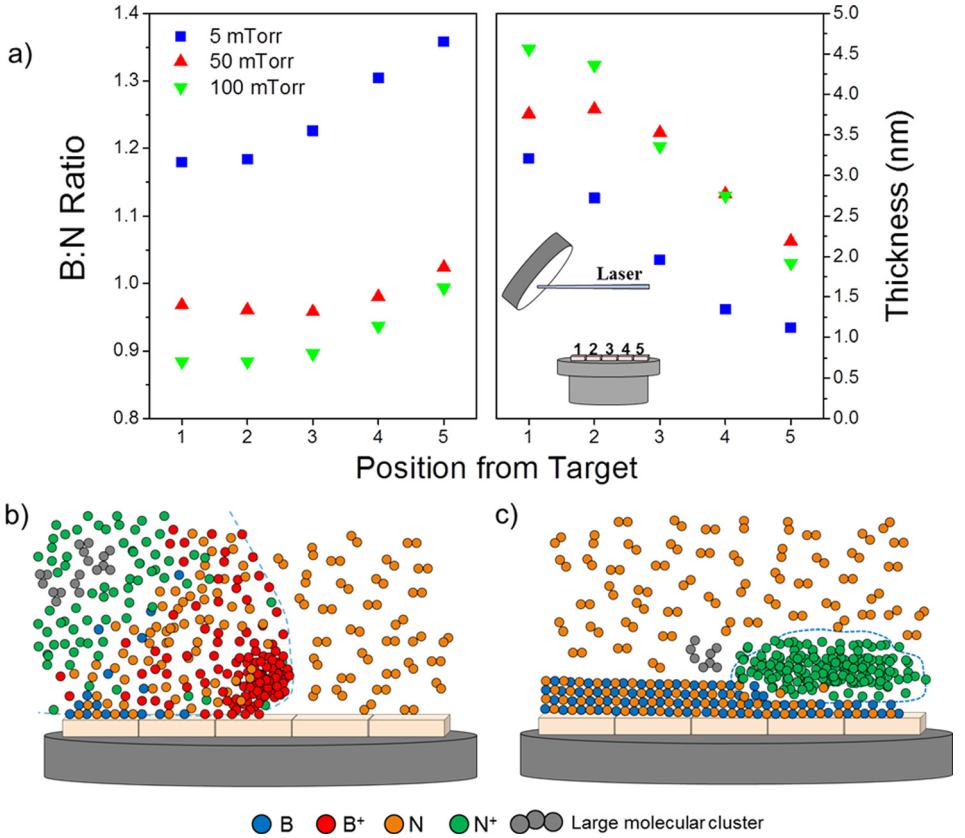


FIG. 8. (a) BN ratio and thickness of laser ablated films grown on five sapphire [0001] substrates at different distances from the target at 5 mTorr, 50 mTorr, and 100 mTorr; (b) schematics of plasma plume compositions at approximately 3000 ns; and (c) 6000 ns after laser pulse.

nitrogen, and therefore can condense and react with the boron at the growth surface for several hundred nanoseconds before a high concentration of $N^+$ is present.

The thickness of the 10 laser pulse ultra-thin BN films varies across the substrate area, shown in Figure 8(a). The higher gas pressure in the chamber leads to thicker nanoscale films, and the thickness drops off as the distance away from the target is increased. A variation of more than 2 nm thickness is observed in the 5 mTorr depositions, as the higher energy species lead to a lower reaction time in the gas phase and can cause desorption of the nucleated films. The 50 mTorr deposition condition also leads to a smaller delta in thickness across the substrate holder area. Samples at position 1, 2, and 3 have nearly identical thickness for this optimal pressure, and at location 4 and 5, the extended presence of energetic $N^+$ ions induces significant desorption of nitrogen. This provides a controlled growth of stoichiometric BN and thickness uniformity within 1 nm at 1 $cm^2$ areas at the 1–3 sample location and 50 mTorr pressures of these studies. For all substrate growth locations and nitrogen pressures considered in the current laser ablation plasma study, there was no significant change in the sample surface roughness due to the BN film growth. An average RMS roughness over the sample surface was 0.18 nm as measured by atomic force microscopy (AFM).

Figure 9 presents an example of a cross-sectional transmission electron microscope (TEM) image from a film grown at room temperature when using the optimized plasma plume conditions discussed in this study. High temperature growth and an appropriate surface template (e.g., highly ordered pyrolytic graphite) facilitates the growth of nanocrystalline *h*-BN with structural and electrical properties close to mechanically exfoliated *h*-BN.[6] The ultra-thin amorphous BN film shown in Figure 9 was grown with 5 laser pulses and, consequently, has a thickness of 1.5 nm, corresponding to about 4–5 monolyaer thickness of the crystalline 2D equivalent. This dense and fully stoichiometric BN film extends over the entire macroscopic sample area and has a very clean and damage free interface with the underlying sapphire, indicating a negligible impact of the energetic species in laser ablated plasma on the substrate surface. These characteristics and the low temperature growth open new opportunities for integrations of ultra-thin PLD grown BN films in 2D electronic device architectures.

To help correlate the ablated plasma studies with possible growth mechanisms of the ultra-thin amorphous BN films, schematics of plasma plume species concentrations and spatial distributions near the substrate surface are shown in Figures 8(b) and 8(c) at approximately 3000 ns and 6000 ns after the laser impacts the target. At 3000 ns, the boron and

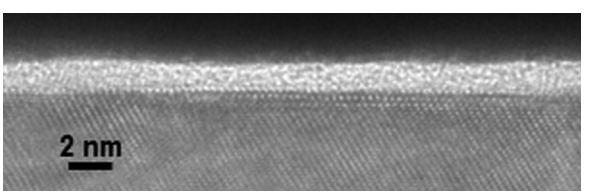


FIG. 9. Example of a cross sectional TEM image of an amorphous BN film grown at room temperature on the top of a sapphire substrate at 50 mTorr nitrogen background pressure. The shown film morphology and thickness uniformity extends microscopically over the entire 5 mm length of the sample.

neutral nitrogen species are heavily concentrated at the front of the plume, as boron reaches the sample first followed by the nitrogen. Molecular boron nitride, BN, is formed mostly at the interface but is represented within the plume at small concentrations. The ionized nitrogen forms from the laser ablation process, as some of the $N^+$ is present at the front of the plume, but most is localized behind the front of the plume. Large molecular clusters formed by laser ablation are hypothesized to follow behind the front of the plume as well, but are typically not detected in plasma emission studies. The collisions with the large molecular clusters with other molecules and with the background gas species happen readily and frequently, as the collisional cross section is significantly higher than the atomic species. These collisions will lead to further creation of $N^+$ at the back of the plume.

One of the major advantages in physical vapor deposition growth of 2D materials is the potential to scale up, as the film coverage is wide-spread over the sample surface, which is required for most industrial applications. In large scale dielectric growth of these films, the sample is rotated and is typically at elevated temperature, which can mitigate the non-uniformity in film thickness and B:N ratio that is observed in these studies.[6] Plasma spectroscopy techniques discussed here can be used to optimize the growth of ultra-thin dense amorphous BN films and provide insights into laser ablation processing of 2D insulating materials.

## CONCLUSIONS

Temporally and spatially resolved spectroscopy, coupled with emission wavelength specific imaging of plasma plumes produced by laser ablation of a BN target in vacuum and background nitrogen, was used to identify and track the evolution of ionized and neutral atomic boron and nitrogen as well as molecular $N_2$, $N_2^+$, and BN from the initial laser-target interaction to the location of condensation at the substrate surface. During initial plume formation, the ablated plasma composition is independent of the background gas pressure and originates from laser ablation of the BN target itself. However, as the plume expands from the target, the shockwave front formation and collisional interactions with the background result in ionized boron and nitrogen concentrations increased by about 140 and 30 times, respectively. The emission enhancement from neutral atomic species is impacted to a lesser degree by the background gas presence with about 7 times intensity increase for neutral nitrogen at the substrate location.

Independent of the background nitrogen pressure, ionized boron arrives at the substrate location first, followed closely by neutral nitrogen. The concentration of ionized boron species increases with pressure due to molecular collisions, and the neutral nitrogen concentration remains approximately constant. Atomic nitrogen ions are generated primarily from dissociation and ionization of the background gas, and majority of $N^+$ ions arrive and dwell at the substrate surface for a few microseconds after neutral B and N species arrive. Molecular ionized nitrogen was also in abundance at the substrate location and showed double maxima intensity behavior as a function of time after the laser pulse. This phenomenon is explained by the background gas first being ionized with a high density electron flux in the front of the ablated plume, and then followed by ionization collisions with the rest of the plume. Presence of molecular BN was identified, but its intensity was relatively low with a negligible contribution to the film growth.

The performed studies helped to identify that a predominant mechanism for BN film formation is condensation surface recombination of boron ions and neutral atomic nitrogen species arriving nearly simultaneously to the substrate location, and that this process occurs before arrival of the majority of $N^+$ ions generated by plume collisions with background nitrogen. Furthermore, the energetic nature and dwelling of incident $N^+$ ions at the substrate location can negatively impact both BN film stoichiometry and thickness. At substrate locations further away from the ablation target where these energetic ions are prevalent, film desorption was linked to the extended $N^+$ bombardment. Growth of stoichiometric and ultra-thin BN films was optimized at enriched concentrations of ionized boron and neutral atomic nitrogen at condensation surfaces. For the plasma–substrate geometry of the present studies, these conditions were at 50 mTorr nitrogen pressure, providing few nanometer thick films with 1:1 BN stoichiometry and good thicknesses uniformity. This study will help direct PLD plasma phenomena in the optimization of stoichiometric BN film growth in both amorphous and hexagonal phases that is a significant addition to the expanding suite of new PVD techniques for 2D heterostructure and device processing.

## ACKNOWLEDGMENTS

The authors would like to thank the support of Arthur Safriet and John Bultman of University of Dayton Research Institute, and Rachel Naguy of SOCHE Laboratories. TSF thanks support by the U.S. National Science Foundation through its Scalable Nanomanufacturing program. Financial support from the Air Force Office of Scientific Research Aerospace Materials for Extreme Environments Program (14RX13COR) is gratefully acknowledged.

[1]A. K. Geim and I. V. Grigorieva, "Van der Waals heterostructures," Nature **499**(7459), 419–425 (2013).
[2]S. Das, R. Gulotty, A. V. Sumant, and A. Roelofs, "All two-dimensional, flexible, transparent, and thinnest thin film transistor," Nano Lett. **14**(5), 2861–2866 (2014).
[3]T. Roy, M. Tosun, J. S. Kang, A. B. Sachid, S. B. Desai, M. Hettick, C. C. Hu, and A. Javey, "Field-effect transistors built from all two-dimensional material components," ACS Nano **8**(6), 6259–6264 (2014).
[4]A. M. Van der Zande, P. Y. Huang, D. A. Chenet, T. C. Berkelbach, Y. You, G. H. Lee, T. F. Heinz, D. R. Reichman, D. A. Muller, and J. C. Hone, "Grains and grain boundaries in highly crystalline monolayer molybdenum disulphide," Nat. Mater. **12**(6), 554–561 (2013).
[5]C. Muratore, J. J. Hu, B. Wang, M. A. Haque, J. E. Bultman, M. L. Jespersen, P. J. Shamberger, M. E. McConney, R. D. Naguy, and A. A. Voevodin, "Continuous ultra-thin $MoS_2$ films grown by low-temperature physical vapor deposition," Appl. Phys. Lett. **104**, 261604 (2014).
[6]N. R. Glavin, M. L. Jespersen, M. H. Check, J. Hu, A. M. Hilton, T. S. Fisher, and A. A. Voevodin, Thin Solid Films **572**, 245–250 (2014).
[7]P. S. Wei, D. J. Nelson, and R. B. Hall, "Laser-induced evaporation of solid surfaces," J. Chem. Phys. **62**(8), 3050 (1975).
[8]P. T. Murray, M. S. Donley, and N. T. McDevitt, "Growth of stoichiometric BN films by pulsed laser evaporation," in *Processing and*

*Characterization of Materials Using Ion Beams*, edited by L. E. Rehn, J. E. Greene, and F. A. Smidt (MRS Proceedings, 1989), pp. 469–474.
[9]G. L. Doll, J. A. Sell, L. Salamanca-riba, and A. K. Ballal, *Laser Deposited Cubic Boron Nitride Films*, edited by D. C. Paine and J. C. Bravman (MRS Proceedings, 1990), pp. 55–59.
[10]K. B. Shin, S. M. Park, and Y. M. Kim, "Pulsed laser ablation of boron nitride," in *Advanced Laser Processing of Materials—Fundamentals and Applications*, 397th ed., edited by R. Singh, D. Norton, L. Laude, J. Narayan, and J. Cheung (Mater. Res. Soc. Symp. Proc., 1995), pp. 265–270.
[11]B. Angleraud, C. Girault, C. Champeaux, F. Garrelie, C. Germain, and A. Catherinot, "Study of the expansion of the laser ablation plume above a boron nitride target," Appl. Surf. Sci. **96–98**, 117–121 (1996).
[12]C. Dutouquet, S. Acquaviva, and J. Hermann, "Detection of boron nitride radicals by emission spectroscopy in a laser-induced plasma," Spectrochim. Acta B **56**, 629–635 (2001).
[13]R. M. Chrenko, "Ultraviolet and infrared spectra of cubic boron nitride," Solid State Commun. **14**(6), 511–515 (1974).
[14]G. A. Slack, "Nonmetallic crystals with high thermal conductivity," J. Phys. Chem. Solids **34**(2), 321–335 (1973).
[15]N. Acacia, E. Fazio, F. Neri, P. M. Ossi, S. Trusso, and N. Santo, "Pulsed laser deposition of boron nitride thin films," Radiat. Effects Defects Solids **163**(4–6), 293–298 (2008).
[16]L. Britnell, R. V. Gorbachev, R. Jalil, B. D. Belle, F. Schedin, M. I. Katsnelson, L. Eaves, S. V. Morozov, A. S. Mayorov, N. M. R. Peres, A. H. Castro Neto, J. Leist, A. K. Geim, L. A. Ponomarenko, and K. S. Novoselov, "Electron tunneling through ultrathin boron nitride crystalline barriers," Nano Lett. **12**(3), 1707–1710 (2012).
[17]NIST Atomic Spectra Database Lines Form, 9–16–2014, available at http://physics.nist.gov/PhysRefData/ASD/lines_form.html.
[18]R. W. Pearse and A. G. Gaydon, *The Identification of Molecular Spectra*, 3rd ed. (Chapman and Hall Ltd, London, 1963).
[19]K. C. Smith, D. A. Saenz, D. Zemlyanov, and A. A. Voevodin, XPS Thickness Solver, 2014.
[20]C. J. Powell and A. Jablonski, *NIST Electron Inelastic-Mean-Free-Path Database* (National Institute of Standards and Technology, Gaithersburg, MD, 2010), Version 1.2, SRD 71.
[21]T. Atwee, L. Aschke, and H. J. Kunze, "Investigations of laser-produced plasmas from boron nitride targets," J. Phys. D **33**(18), 2263–2267 (2000).
[22]C. Muratore, S. G. Walton, D. Leonhardt, R. F. Fernsler, D. D. Blackwell, and R. A. Meger, "Effect of plasma flux composition on the nitriding rate of stainless steel," J. Vac. Sci. Technol. A **22**(4), 1530–1535 (2004).
[23]F. J. Mehr and M. A. Biondi, "Electron temperature dependence of recombination of O2+ and N2+ ions with electrons," Phys. Rev. **181**(1), 264 (1969).
[24]S. Rajendiran, A. K. Rossall, A. Gibson, and E. Wagenaars, "Modelling of laser ablation and reactive oxygen plasmas for pulsed laser deposition of zinc oxide," Surf. Coat. Technol. **260**, 417–423 (2014).
[25]D. B. Geohegan, "Diagnostics and characteristics of pulsed laser deposition laser plasmas," in *Pulsed Laser Deposition of Thin Films* (John Wiley & Sons, Inc., New York, 1994), pp. 115–165.